Available on CMS information server

CMS NOTE 1998/018

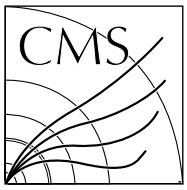

The Compact Muon Solenoid Experiment

CMS Note

Mailing address: CMS CERN, CH-1211 GENEVA 23, Switzerland

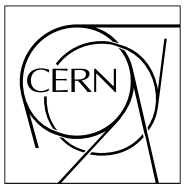

February 23, 1998

Thermal Properties of the Silicon Microstrip Endcap Detector

L. Feld, W. D. Glessing, R. Hammarström

CERN, Geneva, Switzerland

Abstract

Irradiated silicon detectors must be cooled in order to guarantee stable short and long term operation. Using the SiF1 milestone prototype we have performed a detailed analysis of the thermal properties of the silicon microstrip endcap detector. The strongest constraint on the cooling system is shown to be set by the need to avoid thermal runaway of the silicon detectors. We show that, taking into account the radiation damage to the silicon after 10 years of LHC operation and including some safety margin, the detector will need a cooling fluid temperature of around $-20^{\circ}\mathrm{C}$. The highest temperature on the silicon will then be in the range $-15^{\circ}\mathrm{C}$ to $-10^{\circ}\mathrm{C}$. This sets an upper limit on the ambient temperature in the tracker volume.

1 Introduction

The power P_{Si} dissipated by a silicon detector is given by the product of bias voltage U_{bias} and leakage current I_{leak}:

$$P_{Si} = U_{bias} I_{leak}. \tag{1}$$

For a satisfactory detector performance the bias voltage has to be significantly above the depletion voltage U_{dep}. It has been shown (see e. g. [1]) that after type inversion the depletion voltage rises linearly with the irradiation dose and reaches several hundred volts after 10 years of LHC operation. Furthermore, the effect of reverse annealing can lead to a steep increase of the depletion voltage with time. This, however, can be avoided if the silicon detectors are permanently kept at temperatures below $\approx 0°\mathrm{C}$, which sets the first limit on the cooling system for the silicon tracker. It will be shown that during detector operation there are even stronger limits on the silicon temperature. Nevertheless, this limit is very restrictive as it has to be ensured also during the shutdown of the experiment (with possible short warm up periods for repair work).

The leakage current increases with irradiation dose. For the bulk leakage current, which is the dominant contribution, one finds a linear dependency

$$I_{leak} = \kappa\, \Phi\, V, \qquad \kappa \approx 3.5 \cdot 10^{-17}\mathrm{A/cm} \;\; \text{at } 20°\mathrm{C}, \tag{2}$$

where Φ is the particle fluence to which the detector was irradiated and V is the silicon volume. κ is called the leakage current damage constant. The value quoted here was found for a HAMAMATSU detector irradiated with $24\,\mathrm{GeV}/c$ protons at $-5\,°\mathrm{C}$ to a fluence of $1.6 \cdot 10^{14}\mathrm{p/cm}^2$ (value normalized to $20\,°\mathrm{C}$) [2]. After 10 years of LHC operation the inner layers of the silicon microstrip tracker will have received a dose of about $2 \cdot 10^{14}\mathrm{protons/cm}^2$. A typical detector module having a volume of $V = 80\ \mathrm{cm}^2 \times 300\mu\mathrm{m}$ will after this irradiation show a leakage current of around $17\mathrm{mA}$ at $20°\mathrm{C}$.

The leakage current depends strongly on the temperature. Using Boltzmann statistics one derives for the bulk leakage current

$$I_{leak} \sim (kT)^2 \exp\left(-\frac{1.21\ \mathrm{eV}}{2kT}\right), \tag{3}$$

$k = 8.620 \cdot 10^{-5}\ \mathrm{eV/K}$ being Boltzmann's constant and T the temperature of the silicon in degrees Kelvin [3]. In the temperature range of interest this means that the leakage current doubles every $7\,°\mathrm{C}$.

In summary, the power dissipation of an overdepleted silicon detector of $300\ \mu\mathrm{m}$ thickness and $80\ \mathrm{cm}^2$ surface, irradiated with the LHC dose of $2 \cdot 10^{14}\ \mathrm{protons/cm}^2$, can be estimated as

$$P_{Si}(T, U_{bias}) \approx 5000\ \frac{\mathrm{A}}{\mathrm{K}^2} \cdot U_{bias} \cdot T^2 \cdot \exp(-7020.7\,\mathrm{K}/T). \tag{4}$$

In order to limit the shot noise it is necessary to keep the leakage current per strip below $\approx 2\ \mu\mathrm{A}$. After 10 years of LHC operation and assuming 1024 strips on the detector, this translates via eq. 3 into a maximum operating temperature of around $-2\,°\mathrm{C}$. There is, however, another consideration which sets an even lower limit on the operating temperature.

Any cooling system based on heat exchange to a cooling agent, flowing at constant rate, leads to a linear increase of the silicon temperature with the power dissipated in the silicon:

$$\Delta T \equiv T_{Silicon} - T_{CoolingAgent} = \alpha A P_{Si}, \tag{5}$$

α being the heat transfer coefficient and A the effective interfacing area. Thus the detector and its cooling is a non-linear feedback system: an increase in the silicon temperature leads to an increased power dissipation in the silicon (eq. 3) which in turn causes an increase in the silicon temperature (eq. 5) and so on. It has to be ensured that at some temperature this increase in power dissipation is smaller than that which the cooling system can additionally remove. Otherwise the power dissipation of the silicon will quickly rise, a process which is called *thermal runaway* [4]. As the power supply for the bias voltage will probably have a current limit, this event would not necessarily destroy the detector (although there is little experience on this subject). To bring the detector back to operation would, however, require either to decrease the cooling agent temperature or to reduce the bias voltage. For a given cooling system the reduction of temperature is certainly restricted to some practical limits. And a reduction of bias voltage might not be possible given that after type inversion the p^+ on n detectors forseen for CMS need to be well overdepleted to give a decent charge collection performance. It is therefore crucial to avoid thermal runaway and it will be shown that this imposes the strongest requirements on the detector module design and on the cooling system.

2 Hydrodynamic properties of the cooling system

The cooling system forseen for the silicon microstrip tracker of CMS is based on a heat transfer fluid running through a system of small diameter pipes close to the power dissipating parts of the detector, namely the electronics and the silicon itself. In order to describe the characteristics of such a cooling system it is necessary to elaborate on its hydrodynamic properties.

Consider a tube of length l which absorbs a certain power P. The temperature of the fluid at the end of the tube T_{out} is related to the original temperature of the fluid T_{in} by

$$T_{out} = T_{in} + \frac{P}{c_p \rho f}, \tag{6}$$

where c_p is the *heat capacity* $[\mathrm{J}/(\mathrm{kg}\cdot\mathrm{K})]$ and ρ the *density* $[\mathrm{kg}/\mathrm{m}^3]$ of the fluid. f denotes the *volume flow* $[\mathrm{m}^3/\mathrm{s}]$ of the fluid.

There is another temperature gradient which is at least of equal importance, but which is more difficult to calculate. On its way into the fluid the heat has to traverse a layer of laminar flow along the wall of the tube. The rate of this transfer is governed by *Prandlt's number*

$$Pra = \nu \frac{c_p}{\lambda} \rho, \tag{7}$$

which depends on the *heat conductivity* λ $[\mathrm{W}/(\mathrm{m}\cdot\mathrm{K})]$ and the *kinetic viscosity* ν $[\mathrm{m}^2/\mathrm{s}]$ of the fluid as well as on its heat capacity and density. The thickness of this layer depends on the grade of turbulence of the flow which is described by *Reynold's number* Rey, which depends on the diameter of the tube d, the flow f, and the kinetic viscosity ν of the fluid:

$$Rey = \frac{4f}{\pi \nu d}. \tag{8}$$

Empirically one finds that the coefficient for the heat transfer from the wall of the tube into the fluid is given by

$$\alpha_{perp} = 0.023 \cdot Rey^{0.8} \cdot Pra^{0.4} \cdot \frac{\lambda}{d}. \tag{9}$$

The temperature gradient perpendicular to the flow is then

$$\Delta T_{perp} = \frac{P}{A \alpha_{perp}}, \tag{10}$$

A being the effective surface for this transfer.

For the system aspects of the cooling the pressure drop Δp over the pipes is important. One finds

$$\Delta p = \Omega \cdot l \cdot f^2 \quad \text{with} \quad \Omega = \begin{cases} \dfrac{0.31}{Rey^{0.25}} \dfrac{8\rho}{\pi^2 d^5} & \text{if } Rey > 2300 \quad (\text{turbulent flow}) \\ \dfrac{100}{Rey} \dfrac{8\rho}{\pi^2 d^5} & \text{otherwise} \quad (\text{laminar flow}) \end{cases}, \tag{11}$$

where the tube resistance Ω depends strongly on the turbulence of the flow.

2.1 Comparison of different heat transfer fluids

Table 1 shows a comparison of the properties of three heat transfer fluids which might be considered. In the comparison of these fluids the Hydrofluoroether (HFE) has by far the lowest viscosity, which is also quite stable in the range from $+20\ ^\circ\mathrm{C}$ to $-40\ ^\circ\mathrm{C}$. In heat capacity and heat conductivity HFE is, however, inferior to the other fluids. In order to compare the cooling performance of the different fluids one can for a fixed pressure drop derive the resulting flow and the temperature gradients along and perpendicular to the pipe. Assuming a pressure drop of $\Delta p = 1\ \mathrm{bar}$ over a pipe of length $l = 1\ \mathrm{m}$ and inner diameter $d = 0.002\ \mathrm{m}$, one finds the values indcated in table 1. At $+20\ ^\circ\mathrm{C}$ the resulting flow is very similar for all fluids. At $-20\ ^\circ\mathrm{C}$, however, the flow of the ethanol-water mixture is reduced by a factor 10, while the flow for the other fluids does not change very much. The small flow of the ethanol-water mixture at $-20\ ^\circ\mathrm{C}$ implies large temperature gradients along and perpendicular to the pipe, which rules out this fluid for our application. At $-20\ ^\circ\mathrm{C}$ HFE and SYLTHERM show a similar temperature gradient along the pipe, being slightly higher for SYLTHERM. However, in the gradient perpendicular to the pipe the difference is more pronounced, HFE having a temperature gradient which is 30 % smaller than that of SYLTHERM.

product		3M-HFE-7100 $C_4F_9OCH_3$	SYLTHERM XLT Silicon Oil	Ethanol-Water 40:60	units
density ρ	$+20°C$	1506	846	935	kg/m^3
	$-20°C$	1609	881	962	
	$-40°C$	1660	899	974	
viscosity ν	$+20°C$	0.405	1.46	2.9	$10^{-6}\ m^2/s$
	$-20°C$	0.724	3.04	25.3	
	$-40°C$	1.067	4.80	172.	
heat capacity c_p	$+20°C$	1173	1650	4027	$J/(kg \cdot K)$
	$-20°C$	1093	1547	3727	
	$-40°C$	1053	1494	3507	
heat conductivity λ	$+20°C$	0.070	0.111	0.361	$W/(m \cdot K)$
	$-20°C$	0.078	0.119	0.344	
	$-40°C$	0.082	0.123	0.336	
vapour pressure	$+20°C$	0.21	*negligible*		bar
	$-20°C$	0.03	*negligible*		
	$-40°C$	0.009	*negligible*		
residue		< 2.0	10^6		ppm
cost		≈ 100	≈ 100		CHF/liter
for $\Delta p = 1$ bar, $l = 1$ m and $d = 2$ mm:					
flow	$+20°C$	0.58	0.67	0.56	l/min
	$-20°C$	0.52	0.56	0.06	
	$-40°C$	0.48	0.35	0.01	
$(T_{out} - T_{in})/P$	$+20°C$	0.058	0.064	0.029	K/W
	$-20°C$	0.066	0.078	0.270	
	$-40°C$	0.072	0.128	1.952	
$\Delta T_{perp} \cdot A/P$	$+20°C$	2.2	2.7	1.4	$10^{-4}m^2K/W$
	$-20°C$	2.9	4.1	20.1	
	$-40°C$	3.5	7.1	209.	

Table 1: Comparison of different cooling fluids. The value of the heat capacity for 3M-HFE-7100, quoted here from the company's specifications, is inconsistent with our measurements which give $c_p = (1555 \pm 70)\ J/(kg \cdot K)$ at $\approx 23\ °C$. Assuming this value one finds $(T_{out} - T_{in})/P = 0.044(0.050, 0.054)\ K/W$ and $\Delta T_{perp} \cdot A/P = 2.0(2.6, 3.1)\ 10^{-4}m^2K/W$ at $+20\ °C(-20\ °C, -40\ °C)$.

Our own measurement of the heat capacity of 3M-HFE-7100 gave a value which is $\approx\ 30\ \%$ higher than the specifications. Assuming this value, the temperature gradients for HFE are even smaller.

As can be seen from the table, there is no dramatic change in the properties of HFE even down to $-40\ °C$ (the freeze point is $-153\ °C$). This means that a cooling system based on HFE is quite flexible in terms of operating temperature.

Another advantage of HFE is the fact that it evaporates quickly and leaves a very small residue. Actually, HFE is commercially used as cleaning agent. A small leak in a cooling system filled with HFE would most likely not damage other components and the quantity of fluid lost would evaporate. On the other hand the SYLTHERM silicon oil does not evaporate and is very difficult to remove. Given the above, 3M-HFE-7100 is our best candidate for the cooling fluid of the silicon microstrip tracker.

3 Experimental Setup

For the experimental study on the thermal and hydrodynamic properties of the silicon microstrip endcap detector we have used the milestone prototype. It represents a full size prototype of one of the disks in their V2 layout. Thus these test are considered to be made under conditions which are very similar to the situation in the real experiment.

The layout of the disk and the detector modules was based on earlier simulation work and on measurements on smaller test structures [5]. The results of these studies are in good agreement with the measurements on the full size structure presented in this note.

Fig. 1 shows a sketch of the test detector module which was used for these studies. Two dummy detector wafers are

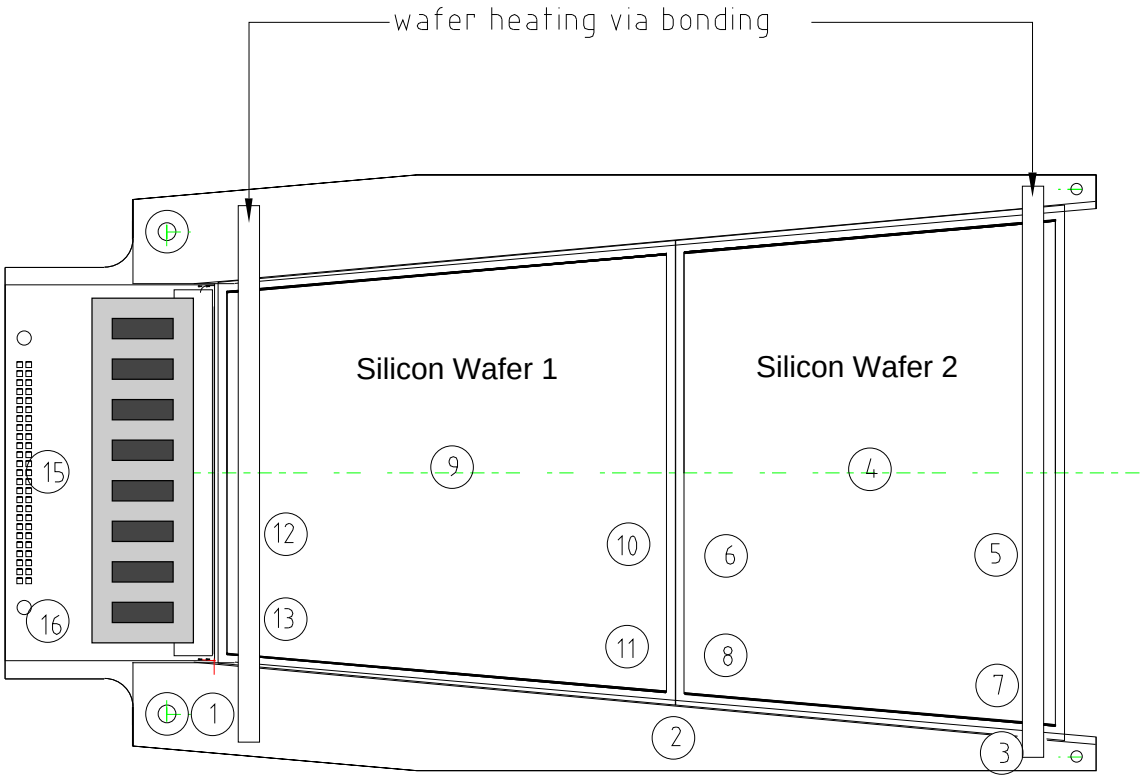

Figure 1: Layout of the test module used for the temperature measurements. Two dummy detector wafers are glued onto the side rails of a carbon fiber frame using standard epoxy and a layer of Kapton tape. The electronics hybrid, normally located on the hybrid carrier part of the frame, is replaced by a heat load resistor. The module has all the wire bonds of a real module. The power dissipation of the silicon was simulated by feeding a current through the metallization of the strips. The numbers in circles indicate the positions and channel numbers of the thermistors used for the temperature measurements.

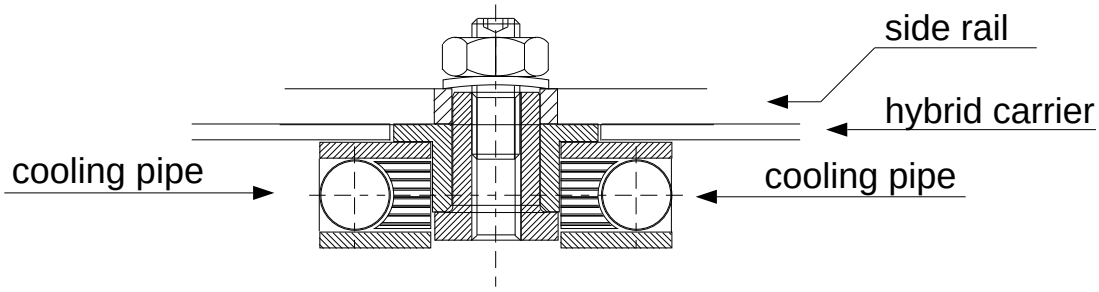

Figure 2: Cross section trough the support ring housing two cooling pipes. The screw clamps the carbon fiber frame of the detector module, consisting of the hybrid carrier and the side rails, onto the ring.

glued onto the side rails of a frame of thermally highly conductive carbon fiber (K1100). Like the real detectors, these wafers are $300\ \mu\mathrm{m}$ thick and have together a surface of about $80\ \mathrm{cm}^2$. In place of the front end electronics hybrid there is a heat load resistor glued onto the hybrid carrier part of the frame. The dummy detectors are wire-bonded to each other and also to the hybrid heat load. Therefore, the thermal properties of this module are very similar to those of a real detector module. The hybrid is expected to dissipate a power of about $2\ \mathrm{W}$ which is simulated by the heat load resistor. The power dissipation of the silicon, which will be of the order of $0.5\ \mathrm{W}$ to $1.0\ \mathrm{W}$ after 10 years of LHC running, is simulated here by feeding a current through the strip metallizations on the dummy detectors. This provides a uniform heat load distribution which is very close to the power dissipation on a real detector. The power dissipated by the hybrid is removed by two cooling tubes which are embedded in a support ring also made of thermally highly conductive carbon fiber (see fig. 2). The module is clamped onto this ring by the screws which are indicated in the figure. The power dissipated in the silicon has to be removed through the side rails either into the two cooling tubes beneath the hybrid or into a third cooling tube to which the

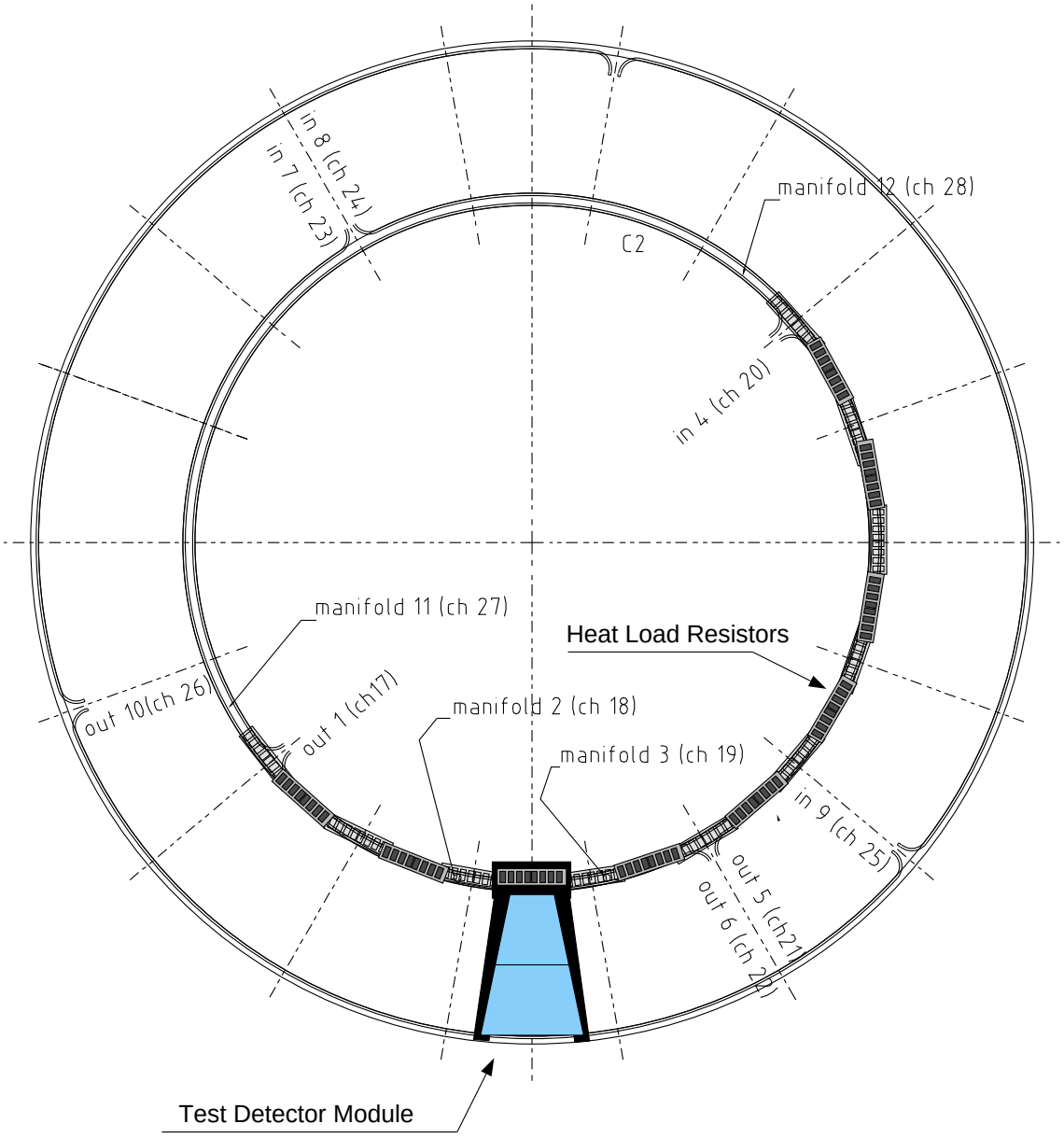

Figure 3: The cooling pipe structure on the milestone prototype disk. Half of the disk is equipped with resistors to simulate the heat load of the detector modules. The test module is mounted at the indicated position. During the measurements those four cooling pipe sections were operated which have contact to either a heat load resistor or the test module.

module is connected at the far end. The junction between the silicon wafers and the carbon fiber frame is delicate. Electrically it has to be a very good insulation as the backplane of the detectors will be operated at high voltage (several hundred volts) while the carbon fiber frame is grounded. Thermally, however, it should of course provide the highest possible conductivity. For the milestone modules (including the test module) this was achieved by inserting a $50\ \mu\mathrm{m}$ layer of Kapton tape between the silicon and the carbon fiber. It should be pointed out that the temperature on the silicon is not only influenced by its own power dissipation. The hybrid contributes by a heat flow through the side rails and through the bond wires.

To obtain detailed information on the temperature distribution on the test module, 16 thermistors were glued onto the module as indicated in the figure. These thermistors (FENWAL, type uni-curve QET, 100 kΩ) have a relative precision of $0.2\,^{\circ}\mathrm{C}$.

Fig. 3 shows the milestone disk with the test module mounted. Three rings of cooling pipes are visible which are subdivided into 2 (3) sectors for the pipes at the inner (outer) radius. The pipes have an outer diameter of $2\ \mathrm{mm}$

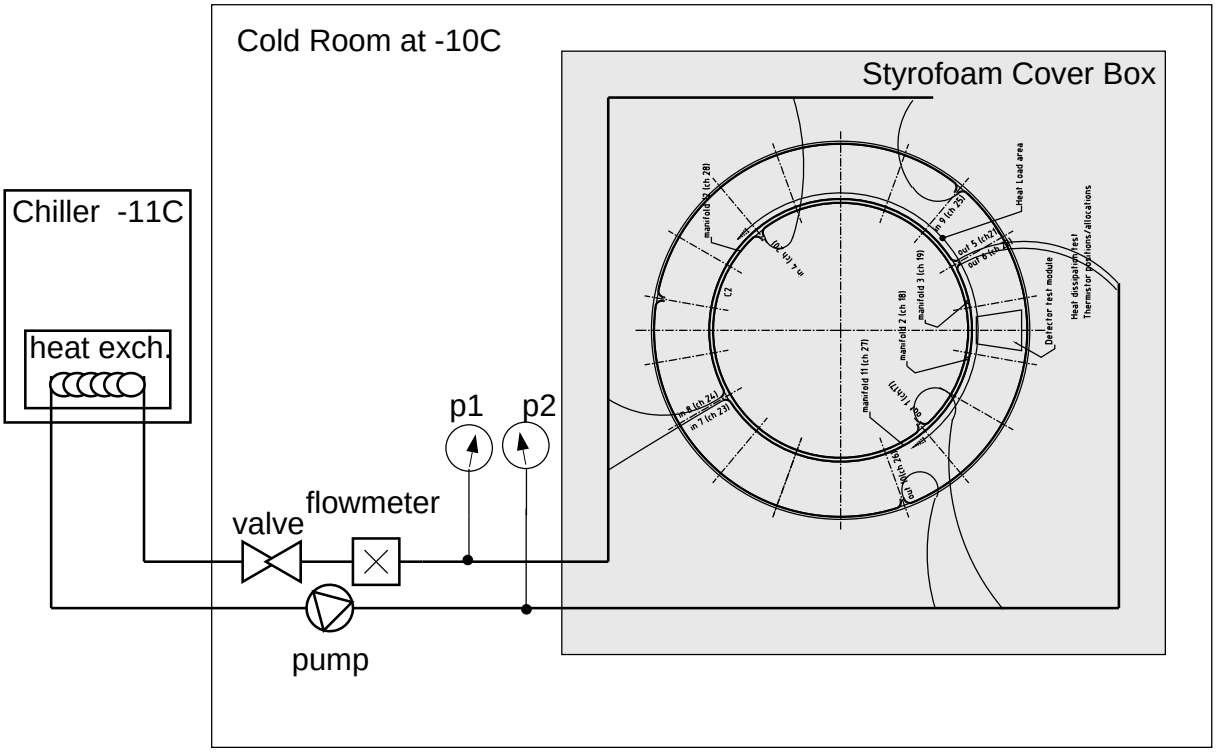

Figure 4: The setup for the temperature measurements. The milestone prototype disk is mounted vertically inside a styrofoam box. Four cooling pipe sections are connected to a primary cooling circuit which is equipped with flow and pressure meters. This whole setup is located in a cold room. The primary cooling circuit is connected via a heat exchanger to a chiller outside the cold room.

and a wall thickness of $30\ \mu\mathrm{m}$. The other detector modules are replaced by heat load resistors (indicated by the grey rectangles), equivalent to that on the test module. They are mounted on the cooling manifold in the positions normally occupied by the module hybrids. Half of the disk is equipped in this way. This implies that four cooling pipe sections have to be operated. A set of 12 thermistors is distributed over the disk to measure the temperature of the incoming and outgoing cooling fluid in the different pipe sectors and the temperatures of the disk at various positions. For the temperature measurements on the test module an estimator for the average fluid temperature is taken to be the mean value of the measurements from channels $17, 20, 22$ and 23.

The disk was mounted vertically in a frame. It was enclosed in a styrofoam box in order to have a defined volume which is decoupled from temperature variations outside the box. The whole setup was installed in a cold room which was operated at $-10\ ^\circ\mathrm{C}$. The detector test module itself was covered on both sides with a Kapton foil in order to minimize convection. All temperature measurements were made after thermal equilibrium was reached.

The input lines to the four cooling pipe sections were connected to a large diameter cooling pipe which itself was instrumented with a pressure-meter and a flow-meter. In the same way the output of the sections was collected in a large diameter pipe instrumented with a second pressure meter. Thus both the total flow and the total pressure drop could be measured. The flows through the four individual sections were adjusted to the same value. This implied insertion of individual constrictors in two of the four pipes which in turn means that the other two pipes already had some internal constriction, i. e. they were not cleaned completely after fabrication of the support ring. The cooling fluid, 3M-HFE-7100, was circulated in a primary circuit which was connected to a chiller unit via a heat exchanger. The temperature of this chiller was set to $-11\ ^\circ\mathrm{C}$. The whole setup is sketched in fig. 4.

4 Measurements of the hydrodynamic properties

A first set of measurements was dedicated to a study of the hydrodynamic properties of the cooling pipes using the 3M-HFE-7100 fluid. Fig. 5 shows the pressure drop over the four parallel cooling pipe sectors as a function of the total flow. The solid line is the prediction from eq. 11 in which the diameter of the tubes was adjusted to fit the points. There is very good agreement for $d \approx 1.5\ \mathrm{mm}$. This is consistent with the fact that all tubes had either some intrinsic constriction or were artificially strangled to obtain the same flow through all pipes (see

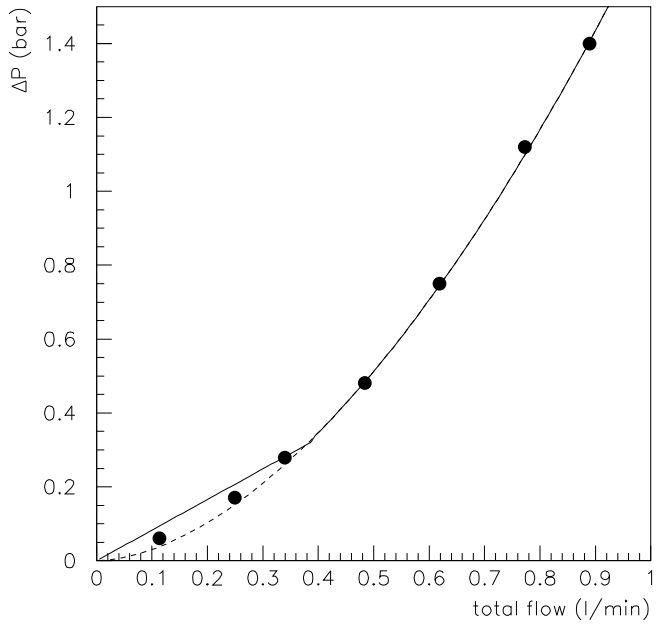

Figure 5: Pressure drop over the cooling pipes as a function of the total flow, for 3M-HFE-7100 at $-10\,^{\circ}\mathrm{C}$. The measurement (dots) is compared to the prediction of eq. 11 (solid line) for an adjusted effective inner tube diameter of $d \approx 1.5\ \mathrm{mm}$. The dashed line indicates the prediction assuming turbulence down to zero flow.

above). The dashed line is the prediction of eq. 11 assuming that the flow is always turbulent. It can be seen that the measurements at small flows are between the two curves. (Without constrictions the tubes with lowest resistance appeared to have an effective diameter of $\approx 1.7\,\mathrm{mm}$.)

As explained in the introduction there are two temperature gradients to be distinguished in the cooling system. The first one is the temperature increase along a pipe which just reflects the power taken away by the heat capacity of the fluid. Fig. 6 (a) shows this temperature increase as a function of the flow for the cooling pipe section which is fully equipped with heat loads. For comparison the curve shows the expectation from eq. 6 which is in good agreement with the measurement. A fluid temperature increase of $2\,^{\circ}\mathrm{C}$, which is considered as the target value, is obtained at a flow of around $0.18\,\mathrm{l/min}$ per pipe. This will be the working point for the following measurements. Taking into account the counter flow in the two cooling pipes underneath the hybrid side of the modules this means that the effective temperature of the fluid at the modules is about $1\,^{\circ}\mathrm{C}$ above its input temperature.

Fig. 6 (b) shows a measurement of the temperature gradient in the fluid perpendicular to the flow. The ΔT shown is the difference between the temperature on the support ring, close to the test module, and the average temperature of the fluid. Thus there is an additional resistance for the heat, which has to traverse the carbon fiber of the support ring before it reaches the wall of the pipe. This modifies the heat transfer coefficient to

$$\alpha = \left(\frac{1}{\alpha_{perp}} + \frac{1}{\alpha_{CarbonFiber}} \right)^{-1} . \tag{12}$$

Using α_{perp} from eq. 9 and assuming $\alpha_{CarbonFiber} = 3000\ \mathrm{W}/(\mathrm{m}^2 \cdot K)$ (according to the thickness of the carbon fiber) results in the prediction shown by the curve in the figure. It is in good agreement with the measurements. For the flow of $0.18\,\mathrm{l/min}$ per pipe (working point) the gradient from the fluid to the carbon fiber manifold is around $3\,^{\circ}\mathrm{C}$.

Summarizing these two contributions, the surface to which the detector modules are attached is around $4\,^{\circ}\mathrm{C}$ warmer than the input cooling fluid temperature for a power dissipation of $2\ \mathrm{W}$ on each hybrid and $0.5\ \mathrm{W}$ on the silicon.

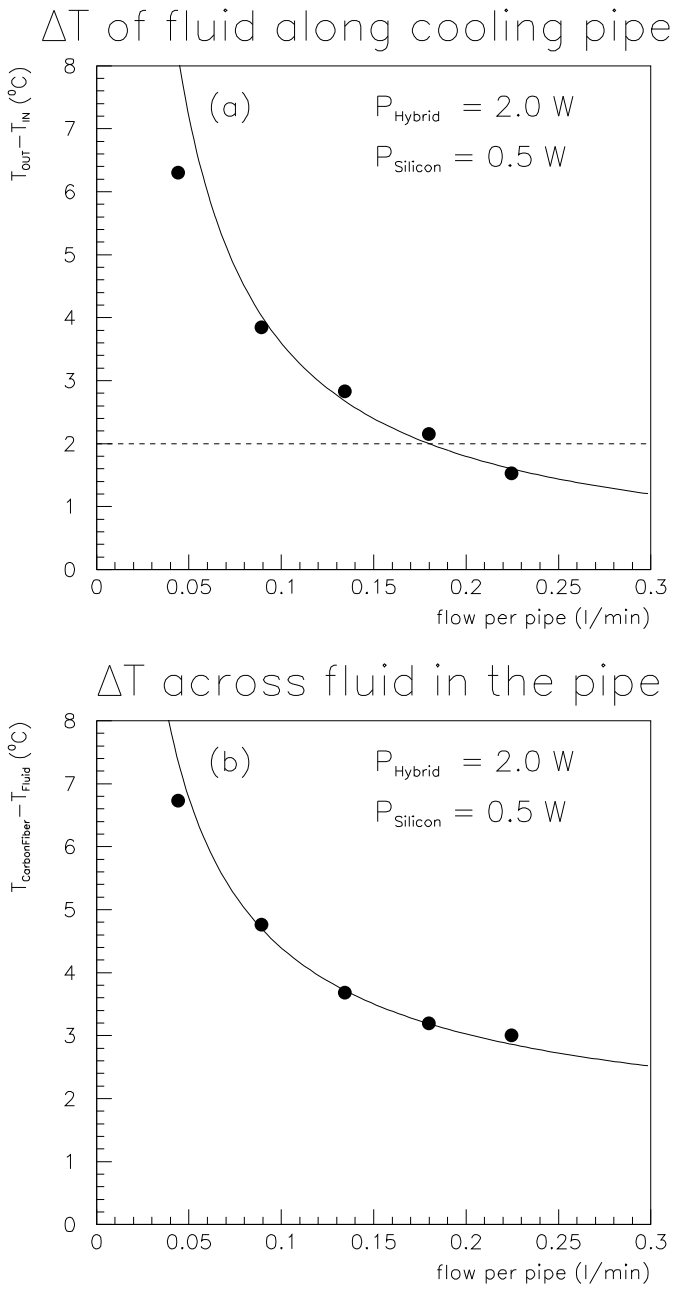

Figure 6: (a) Temperature increase along the cooling pipe section fully equipped with heat loads as a function of the flow at a power dissipation of 2 W on the hybrids and 0.5 W in the silicon. The solid line shows the prediction of eq. 6, assuming that 14 W are absorbed by this pipe, which is a reasonable value taking into account the regions of overlap and the direction of flow of the pipe w. r. t. the other pipes. (b) Temperature gradient in the fluid perpendicular to the flow. For details see text. Both measurements were made with the 3M-HFE-7100 cooling fluid at $-10\,^{\circ}\mathrm{C}$.

5 Thermal properties of the detector module

Fig. 7 shows the temperature distribution on the detector module for a power dissipation of 2 W on the hybrid and 0.5 W on the silicon. The bigger numbers give the difference between the temperature measured at the indicated location and the average cooling fluid temperature. The smaller numbers give the corresponding thermistor channel number. The temperature is highest on the hybrid reaching about $8\ ^\circ$C above coolant temperature. On the silicon one finds a superposition of two gradients. One is due to the heat flow from the center of the silicon to the side rails. It is of the order of a few tenths of a degree. The other reflects the heat flow from the hybrid into the silicon. This is a rather big effect as one can see by comparing the two silicon wafers. The edge of the silicon close to the hybrid is about $2.5\ ^\circ$C warmer than the far end of the silicon. The temperature step due to the transfer of heat from the silicon into the side rails amounts to about $1.5\ ^\circ$C.

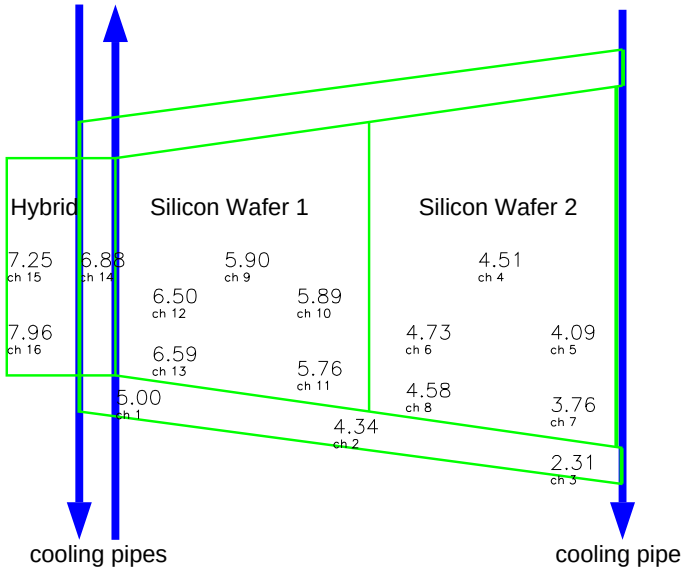

Figure 7: Temperature distribution on the detector module for a power dissipation of 2 W on the hybrid and 0.5 W on the silicon. The bigger numbers give the difference of the temperature measured at the indicated position to the average cooling fluid temperature while the smaller numbers give the thermistor channel numbers.

In order to evaluate the equilibrium temperature that will be reached on a real detector module it is necessary to evaluate the slope of the increase in temperature with power dissipation and also the offset in temperature on the silicon due to the influence from the hybrid. The slope is directly connected to the heat flow coefficient for the path from the location of the measurement to the coolant. For this purpose a set of measurement were made keeping the hybrid power fixed at 2 W and varying the silicon power between 0 W and 1.5 W. Fig. 8 shows the ΔT w. r. t. the average coolant temperature at different points on the module as a function of the power dissipated on the silicon. In (a) the three measurements on the hybrid carrier are shown. As expected they do not depend very much on the power dissipated on the silicon. On the other hand the temperature at the center of the silicon wafers depends strongly on the silicon power (b). A slope of $\frac{dT}{dP} \approx 5$ K/W is found with an offset due to the hybrid power of $4\ ^\circ$C ($2\ ^\circ$C) on the wafer closer to (farther from) the hybrid. Along the edge of the silicon the slopes are slightly more shallow. The offset now depends strongly on the distance to the hybrid, reaching almost $5\ ^\circ$C for channels 12 and 13. The slope of these is $\frac{dT}{dP} \approx 4$ K/W. Finally, (d) contains the measurements made on the side rail. Here the slopes are more shallow, reflecting the fact that a significant fraction of the resistance of the heat path from the silicon to the coolant is due to the transition from the silicon into the side rails. Table 2 summarizes the measurements for all measurement points on the module. Combining these measurements in taking the worst values for the slope and the offset we derive as the highest temperature on the silicon for a given power dissipation by the hybrid and the silicon:

$$T_{Si} = 5.5\ \frac{\mathrm{K}}{\mathrm{W}} \cdot P_{Si} + 2.5\ \frac{\mathrm{K}}{\mathrm{W}} \cdot P_{Hyb} + T_{coolant}. \tag{13}$$

This overestimates the temperature slightly as the largest slope and offset are seen at different points on the silicon.

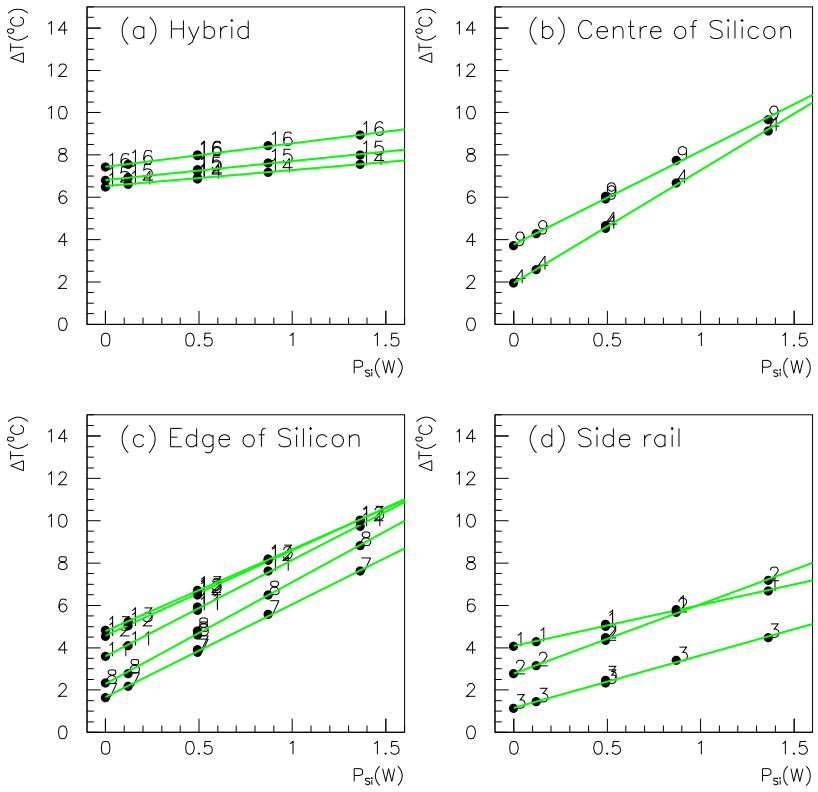

Figure 8: Temperatures measured at various positions on the module relative to the average cooling fluid temperature as a function of the power dissipation of the silicon for a fixed hybrid power of 2 W.

Thermistor	Location	$\frac{dT}{dP_{Si}}$ (K/W)	$\frac{dT}{dP_{Hyb}}$ (K/W)
1	side rail	1.9	2.0
2	side rail	3.3	1.4
3	side rail	2.5	0.6
4	centre of silicon	5.3	1.0
5	edge of silicon	5.0	0.9
6	silicon	5.5	1.1
7	edge of silicon	4.4	0.8
8	edge of silicon	4.8	1.1
9	centre of silicon	4.4	1.9
10	silicon	4.9	1.8
11	edge of silicon	4.6	1.8
12	edge of silicon	4.0	2.3
13	edge of silicon	3.9	2.4
14	hybrid	0.8	3.3
15	hybrid	0.9	3.4
16	hybrid	1.1	3.7

Table 2: Scaling factors of the temperature at the various positions on the module with the power dissipation of the silicon and of the hybrid.

6 Temperature on the silicon during detector operation

As mentioned in the introduction, the temperature of the silicon during detector operation is the result of the balance between its power dissipation (eq. 4) and the power absorption of the cooling system (eq. 13) at that temperature.

We assume a power dissipation by the silicon as given by eq. 4 at a bias voltage of $U_{bias} = 500$ V and a cooling performance as given by eq. 13 at a hybrid power dissipation of 2 W. Fig. 9 (a) shows that for a coolant temperature of $0\,^\circ$C the system is unstable. When the bias voltage is switched on the silicon has a temperature of $5\,^\circ$C due to the heat load from the hybrid. At this temperature the silicon dissipates a power of around 2 W. For this power

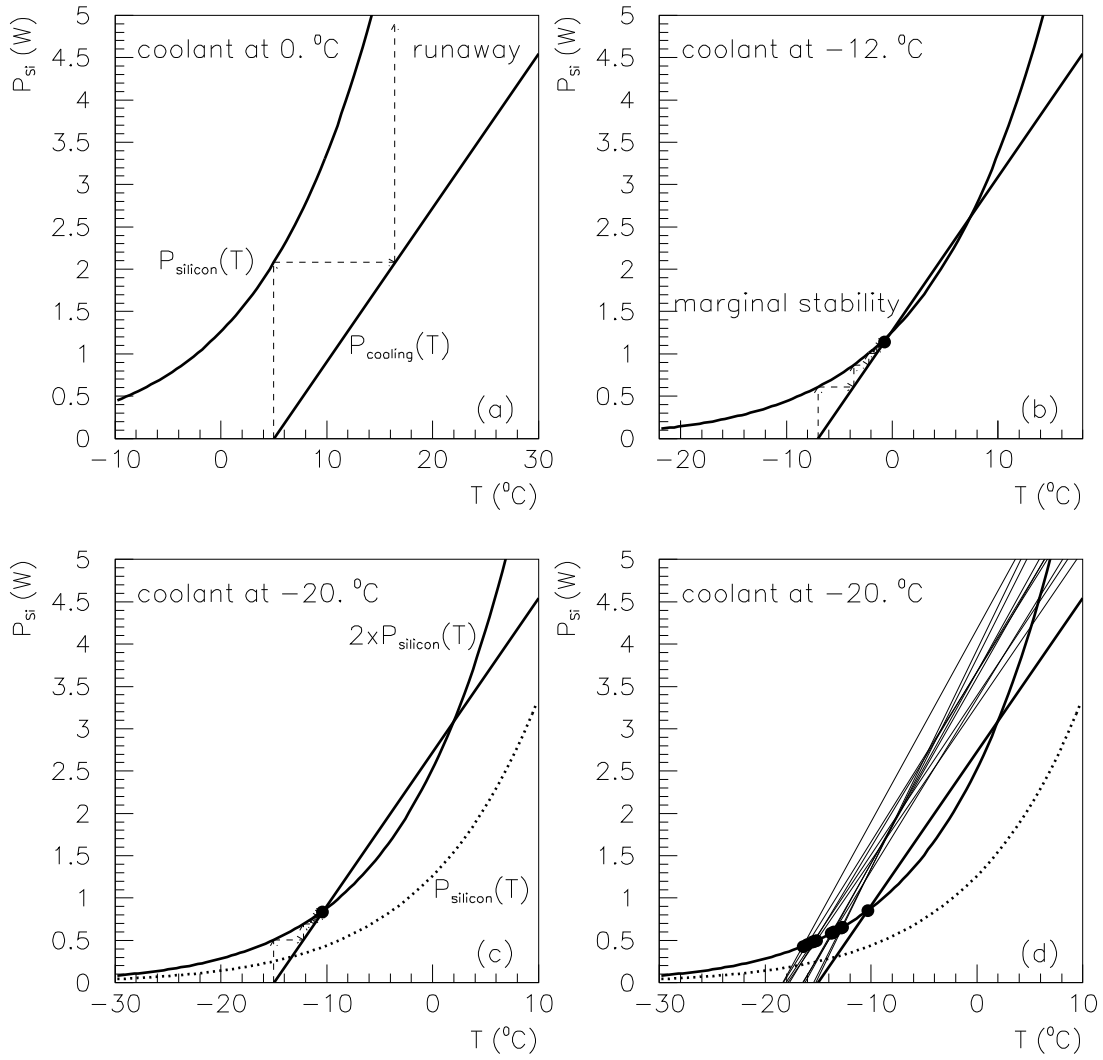

Figure 9: Silicon temperature for different operating conditions. The thick curve shows the power dissipation of the silicon as a function of temperature (eq. 4), assuming a bias voltage of $U_{bias} = 500$ V. The thick line shows the power that the cooling system removes for a given temperature on the silicon (eq. 13). A hybrid power dissipation of 2 W is assumed. (a) coolant temperature $0\,^\circ$C: the silicon temperature increases steadily (thermal runaway), (b) coolant temperature $-12\,^\circ$C: the equilibrium temperature of the silicon is slightly below $0\,^\circ$C, the stability is marginal, (c) assuming twice the power dissipation of the silicon and a coolant temperature of $-20\,^\circ$C: the equilibrium temperature of the silicon is around $-10\,^\circ$C (for comparison the nominal power dissipation of the silicon is shown as the dotted line), (d) same as (c), but now the (thin) lines for all the measurement points on the silicon are included.

we find that the silicon heats up to $16\,^{\circ}\mathrm{C}$, causing in turn an even higher power dissipation. We observe thermal runaway. When the coolant temperature is decreased to $-12\,^{\circ}\mathrm{C}$ (b) a point of equilibrium is reached slightly below $0\,^{\circ}\mathrm{C}$. This is just what is required to avoid reverse annealing of the irradiated silicon. But the stability is quite marginal. Furthermore, one would like to include some safety margin. Therefore, we now assume (for fig. 9 (c) and (d)) a power dissipation of the silicon which is twice as high as expected from eq. 4. For a coolant temperature of $-20\,^{\circ}\mathrm{C}$ the silicon then reaches an equilibrium temperature of around $-10\,^{\circ}\mathrm{C}$.

The (thick) lines shown in fig. 9 (a)-(c) correspond to eq. 13, which represents a combination of the worst dT/dP slope and the worst temperature offset due to the hybrid heat load seen in the measurements on the silicon. The (thin) lines for the 10 points on the silicon where measurements were actually made are included in (d), which is otherwise identical to (c). We see that the hottest of these points would reach $-12\,^{\circ}\mathrm{C}$, i. e. slightly less than for the reference line. At nominal power dissipation of the silicon (dotted line) the hottest point reaches around $-14\,^{\circ}\mathrm{C}$.

These studies are summarized in figs. 10 and 11. They show the equilibrium temperature of the silicon (encoded by the different shadings) as a function of the coolant temperature. In fig. 10 the power dissipation of the silicon is scaled along the ordinate w. r. t. the nominal power dissipation (eq. 4). In this way one can see what the effect of a possible deviation from the leakage current damage constant (eq. 2) or a change in bias voltage would be. According to eq. 13 it also covers a change in the slope dT_{Si}/dP_{Si}. At a coolant temperature of $-20\,^{\circ}\mathrm{C}$ a (combined) increase of these parameters by a factor of two is tolerable without risking thermal runaway.

In fig. 11 the power dissipation of the hybrid is varied along the ordinate. This is important in particular as the 2 W assumed for the hybrid throughout this study might change slightly for the final version of the electronics. The implications of a change in the slope dT_{Si}/dP_{Hyb} can be studied with this plot as well. At a coolant temperature of $-20\,^{\circ}\mathrm{C}$ an increase of the hybrid power up to 4 W (or a corresponding change in the slope dT_{Si}/dP_{Hyb}) seems tolerable.

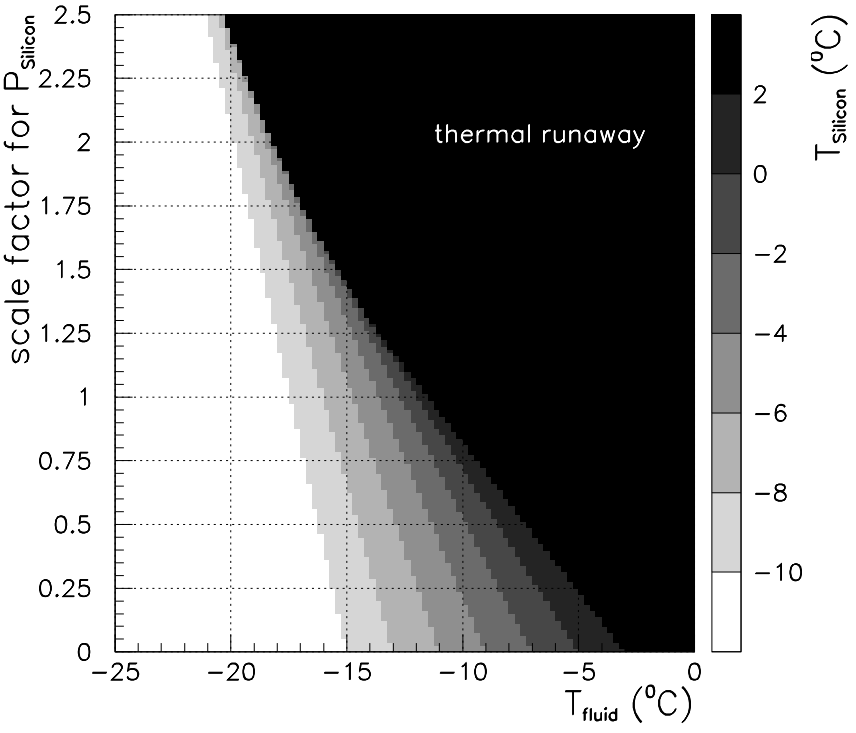

Figure 10: Temperature on the silicon (encoded by the different shadings) resulting from the combination of eq. 13 and eq. 4, assuming a bias voltage of $U_{bias} = 500$ V. Along the abscissa the coolant temperature is varied. Along the ordinate the power dissipation of the silicon is scaled w. r. t. the nominal value of eq. 4. A hybrid power dissipation of 2 W is assumed.

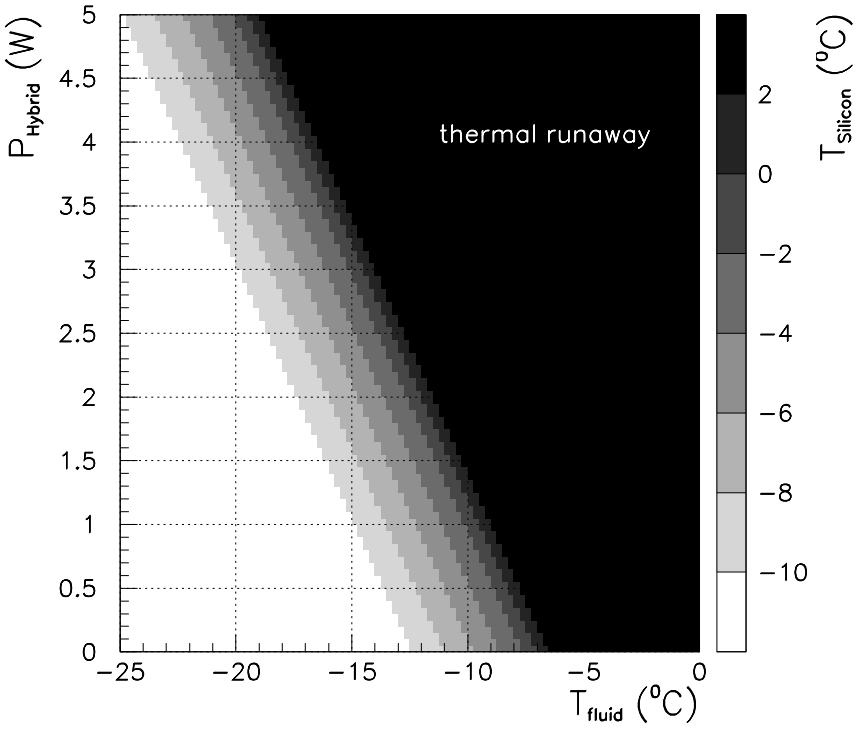

Figure 11: Temperature on the silicon (encoded by the different shadings) resulting from the combination of eq. 13 and eq. 4, assuming a bias voltage of $U_{bias} = 500$ V and the nominal leakage current. Along the abscissa the coolant temperature is varied. Along the ordinate the power dissipation of the hybrid is varied.

Once the equilibrium temperature of the silicon is found one can calculate the corresponding power dissipation of the silicon according to eq. 4. This is shown in figs. 12 and 13.

The silicon detectors have a large surface which will be directly exposed to the atmosphere within the tracker volume. Thus there can be a significant exchange of heat. As additional heat load on the silicon has to be avoided the temperature of the atmosphere must not be higher than the silicon temperature, i. e. not higher than $\approx -10\,^{\circ}\mathrm{C}$. If the atmospheric temperature stays below that of the silicon there will be heat flow from the silicon into the atmosphere by convection and radiation. In our measurements we have minimized convection by a Kapton foil enclosing the module. Thus, an additional convective cooling would result in a better cooling behaviour than obtained here. However, as it is difficult to estimate the effect of this on the thermal behavior of the detector we preferred to take the conservative approach of not including it in our estimations.

7 Summary

We have presented a detailed study of the thermal properties of the silicon microstrip endcap detector using the full size milestone prototype. Using the 3M-HFE-7100 fluid as coolant we have measured the hydrodynamic properties of the cooling tubes and find agreement with expectations. For various simulated heat loads on the silicon and on the hybrid we have measured the temperature distribution on a detector module. From these measurements we can estimate the equilibrium temperatures on the silicon detector under various operating conditions. It is found that a coolant temperature of $-20\,^{\circ}\mathrm{C}$ at the detector module is necessary to safely protect the detectors from thermal runaway, taking into account the radiation damage to the silicon after 10 years of LHC operation. The silicon detectors will then have a maximum temperature of $-15\,^{\circ}\mathrm{C}$ to $-10\,^{\circ}\mathrm{C}$. To avoid additional heat flux into the large surface of the silicon, the atmosphere within the tracker volume must not be warmer than this temperature.

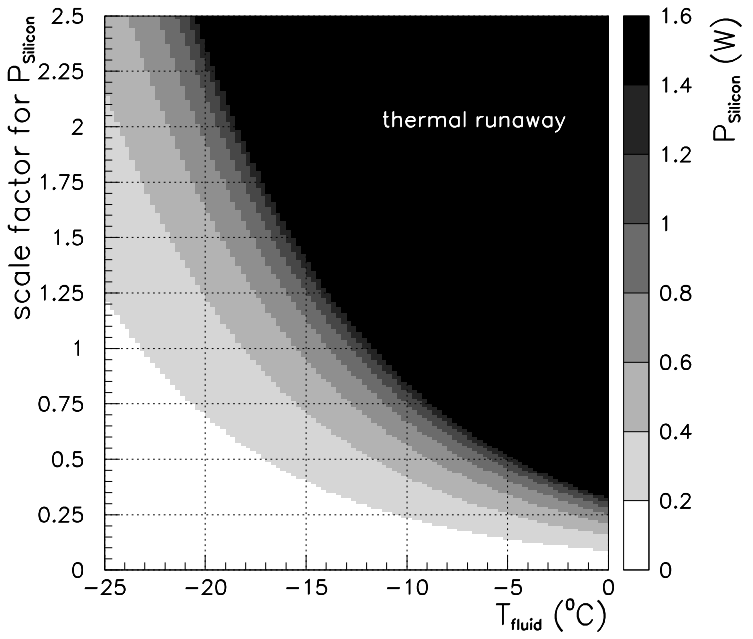

Figure 12: Power dissipation in the silicon (encoded by the different shadings) corresponding to the equilibrium temperatures shown in fig. 10. (The silicon is 300 μm thick and has a surface of 80 cm^2.)

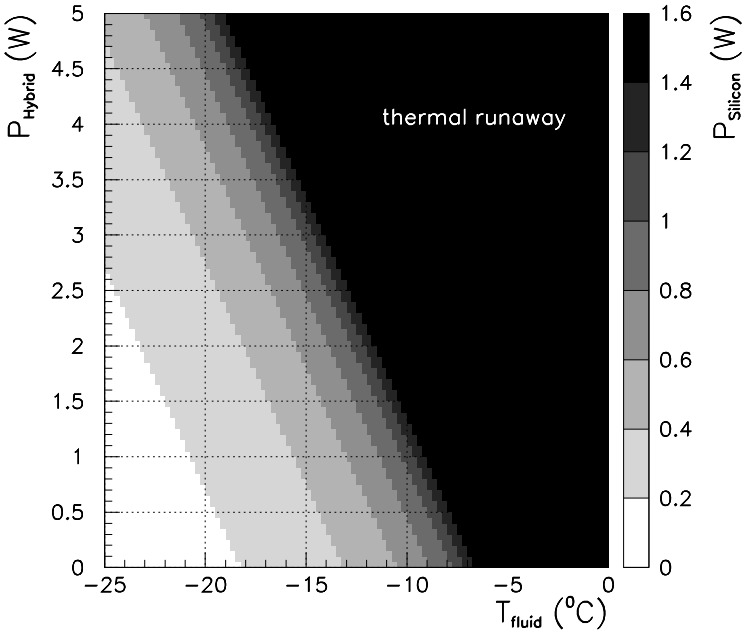

Figure 13: Power dissipation in the silicon (encoded by the different shadings) corresponding to the equilibrium temperatures shown in fig. 11. (The silicon is 300 μm thick and has a surface of 80 cm^2.)

References

[1] F. Lemeilleur et al., 'Study of characteristics of silicon detectors irradiated with 24 GeV/*c* protons between $-20^{\circ}\mathrm{C}$ and $+20^{\circ}\mathrm{C}$', CERN-ECP/94-8, July 21, 1994.

[2] B. Schmitt, to be published in a forthcoming CMS note.

[3] G. Lindström, 'Radiation damage in silicon detectors', SITP Internal Note; February 10, 1991.

[4] T. Kohriki et al., 'First observation on thermal runaway in the radiation damaged silicon detector', KEK Preprint 95-157, November 1995.

[5] CERN and Florence CMS-Si groups, 'SiF1 Milestone Report', presented to the LHCC September 3, 1997.